PAPER

Large improvement in DC electrical properties of EPDM with 2D platelet nanoclay

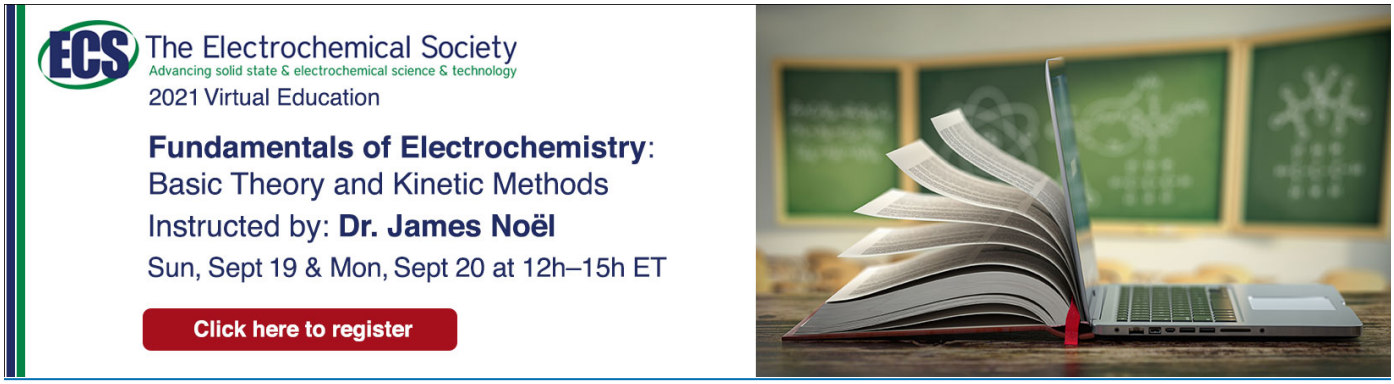

IOP Publishing Journal of Physics D: Applied Physics
J. Phys. D: Appl. Phys. **54** (2021) 475304 (11pp) https://doi.org/10.1088/1361-6463/ac2277

Large improvement in DC electrical properties of EPDM with 2D platelet nanoclay

Mohamadreza Arab Baferani[1,2], Chuangyang Li[2], Mattewos Tefferi[1,2], Ningzhen Wang[2] and Yang Cao[1,2,*]

[1] Department of Electrical and Computer Engineering, University of Connecticut, Storrs, CT 06269, United States of America
[2] Electrical Insulation Research Center, Institute of Materials Science, University of Connecticut, Storrs, CT 06269, United States of America

E-mail: yang.cao@uconn.edu

Received 12 June 2021, revised 23 August 2021
Accepted for publication 31 August 2021
Published 10 September 2021

Abstract

Space charge, electrical conductivity and breakdown strength of polymeric insulations are considered to be the most important characteristics for designing DC cable insulation. In this paper, we report the DC electrical properties of ethylene propylene diene polymethylene (EPDM) polymer with two different 2D inorganic clays, one of which shows large improvement of space charge distribution, controlled electrical conductivity and breakdown voltage. The results revealed that compared with the pure EPDM, the space charge accumulation for EPDM filled with Talc was suppressed significantly, especially at 50 °C with thermal gradient. The maximum local electric field enhancement in the volume decreased from 60% for the pure EPDM to 4% for the Talc-filled EPDM under 20 kV mm^{-1} at 25 °C, while the corresponding value dropped dramatically from 83% to 8% at 50 °C with thermal gradient. Compared with the EPDM, the Talc-filled EPDM showed higher conductivity but with less dependence to electric field and temperature. Microstructure studies suggest the platelet Talc particles distribute in the EPDM matrix homogeneously and make a uniform morphology. This condition consequently causes a desired trap distribution with high density of shallow traps due to the presence of high interfacial area between polymer chains and clay particles which prevents the charge accumulation during the charge carrier transport under DC electric field. Results of the thermally stimulated depolarization current spectra of the samples are in good agreement with the predicted trap distribution based on the experimental results and morphological study.

Keywords: electrical conductivity, EPDM, HVDC cable insulation, space charge accumulation, Talc, Kaolin

(Some figures may appear in colour only in the online journal)

1. Introduction

Ethylene propylene rubber (EPR), due to its excellent electrochemical performance and water-treeing resistant properties, has been used widely as the insulation for AC cables in coal mine, electric power plant, as well as submarine, etc [1–4]. However, under high voltage direct current (HVDC), the desired characteristics for dielectrics are different and low space charge accumulation is preferred, along with other requirements of controlled electrical conductivity and high breakdown strength [5, 6]. As such, EPR shall be properly formulated as a suitable candidate for HVDC cable insulation.

* Author to whom any correspondence should be addressed.

Adding fillers modifies the bulk properties of polymers, which has been accepted as a useful tool to suppress the space charge and to increase breakdown voltage of polymers. So far, various inorganic fillers including SiO_2, ZnO, SiC, TiO_2, MgO, Al_2O_3, hydrated metal oxide, etc, have been used to modify DC electrical properties of polymers such as XLPE, EPR, etc [7–15]. For instance, Roy *et al* studied the effect of silica nanoparticles to enhance DC breakdown strength, and it was shown that adding nanoscale silica particles increases the breakdown strength up to 20% compared to the unfilled XLPE [8]. Literature 11 presented the XLPE/SiC nanocomposites with a concentration of 1 wt% have a higher DC breakdown strength and lower space charge accumulation compared to unfilled XLPE and 3 wt% and 5 wt% filled XLPE. Pallon *et al* clarified that MgO nanoparticles reduce electrical conductivity of LDPE significantly [13]. Literature 14 showed that nano-Al_2O_3 particles can enhance the volume resistivity and suppress space charge of LDPE composite.

Mineral inorganic fillers comparing to synthetic metallic oxide and nonmetallic inorganic oxide fillers used in polymers are more beneficial in terms of lower cost and higher scalability for the large scale manufacturing [16]. In this study, we used 2D Kaolin and Talc clays in ethylene propylene diene polymethylene (EPDM) backbone and found that introducing Talc (magnesium silicate) to EPDM results in a large improvement in space charge accumulation and breakdown voltage of EPDM, while the sample filled with Kaolin (aluminum silicate) showed reduced properties compared with the pure EPDM. It is found that the introduction of the inorganic 2D clays modifies the morphology and trap distribution of the composite dielectric and hence the macroscopic electrical properties.

2. Experimental setup

Two different inorganic platelet nanoclays, i.e. Talc-pyrophyllite magnesiumsilicate and Kaolin-kaolinite aluminiumsilicate, were selected and incorporated to EPDM matrix with a filling ratio of 65 parts per hundred resin (PHR) to prepare EPDM clay nanocomposites. Three samples including EPDM, EPDM filled with Kaolin, and EPDM filled with Talc, named EPDM, $EPDM_{CK}$ and $EPDM_T$, respectively, were prepared and investigated. Test specimens were hot-pressed initially at 130 °C allowing the melting of resin composite under 9 tons of pressure and then cross-linked at 170 °C, followed by cooling down to room temperature under the pressure.

To observe and characterize the morphology of samples and distribution of fillers across the EPDM base polymer, a Thermo Fisher Verios scanning electron microscopy (SEM) was utilized. Thermogravimetric analysis (TGA) was measured by a TGA Q500 V20.13 Build 39 and the differential scanning calorimeter (DSC) were recorded by a DSC Q100 V9.9 Build 303 to study thermal properties of the materials.

The space charge profiling was conducted by the pulsed electroacoustic (PEA) method. For PEA measurement, the specimens were coated on both sides with 60/40 weight% Au/Pd sputter coating with diameter of 1 cm as electrodes. To improve acoustic impedance matching between the sample and the electrodes, a small amount of silicone oil was put between them. A semiconducting (SC) layer was used between the high voltage electrode and the coated sample to minimize the mismatch of acoustic impedance, while the coated specimen was placed directly on the grounding aluminum electrode [2, 6].

The DC conductivity of plaque specimens was measured using a three-terminal sample holder designed according to ASTM 257 specifications. Specimens of 200 μm in thickness were inserted in guarded stainless-steel electrodes for quasi steady-state current measurements by using a Keithley 6517 electrometer for 2000 s. The average reading of the conduction current between 1900 s and 2000 s was used to calculate the electrical conductivity. More details of the space charge and DC conductivity measurements can be found in the previous works [2, 6].

For the DC breakdown strength measurement, the samples were placed in a testing cell with oil along with electrodes in 1 inch diameter. A signal generator provided the ramp waveform to a Spellman high voltage power supply to generate the high voltage ramp breakdown. Five tests were performed for each specimen during the breakdown test. Thermally stimulated depolarization current (TSDC) was measured using a Keithley 6517 electrometer along with a Delta Design 9023 programmable oven to control the heating and cooling processes.

3. Experimental results

Figure 1(a) presents the TGA results, measured with a temperature ramp rate of 20 °C min^{-1} to 600 °C, for the three samples. The base polymer, EPDM, starts to decompose from 300 °C and the maximum decomposition takes place in the range of 400 °C–500 °C. At 500 °C, 100% of unfilled sample and 60% of the filled samples were decomposed. To characterize their thermal behaviors, DSC scans in the following cycles were recorded, including first, a heating run from −50 °C to 200 °C, then, an isothermal condition for 2 min, next, a cooling run from 200 °C to −50 °C, and finally, another heating run from −50 °C to 200 °C. The rate of heat flow during all measurement was 10 °C min^{-1}.

Figures 1(b) and (c) show the cooling and second heating runs in DSC. The glass transition presents with a peak in both of the processes. This should be due to the molecular relaxation which usually appears as a weak endothermic transition in the heating process near the end of a glass transition. Compared to the pure EPDM, the glass transition temperature of the samples with fillers did not change and is around −50 °C, but with lower peak heights than the pure EPDM.

The cross-sectional SEM photos of the three different EPDM samples are shown in figure 2, each in two magnifications. The morphology of cross-linked EPDM without any filler appears homogeneous. However, it can be seen that the shape of fillers and the morphology of organic parts in $EPDM_{CK}$ and $EPDM_T$ are significantly different. Figures 2(c) and (d) demonstrate the distribution of Kaolin particles in

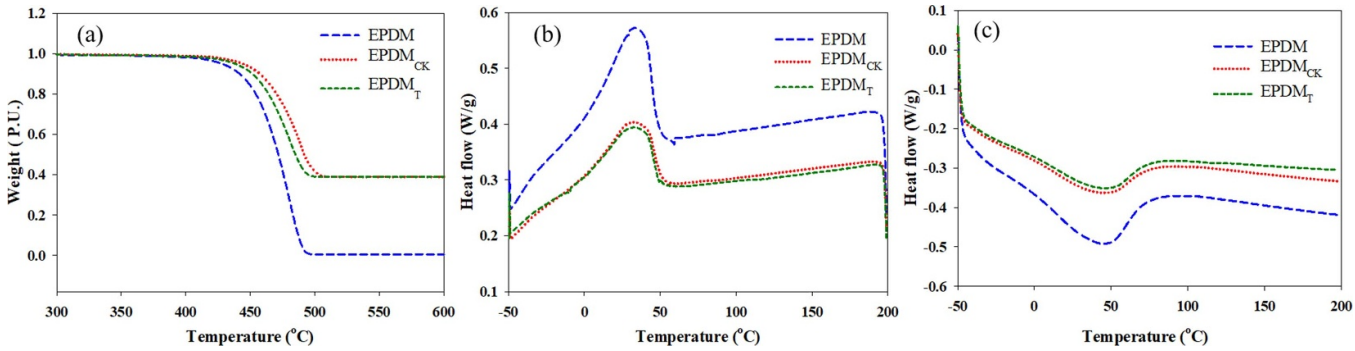

Figure 1. (a) TGA curves (b) the cooling process of DSC and (c) the second heating process of DSC for the samples.

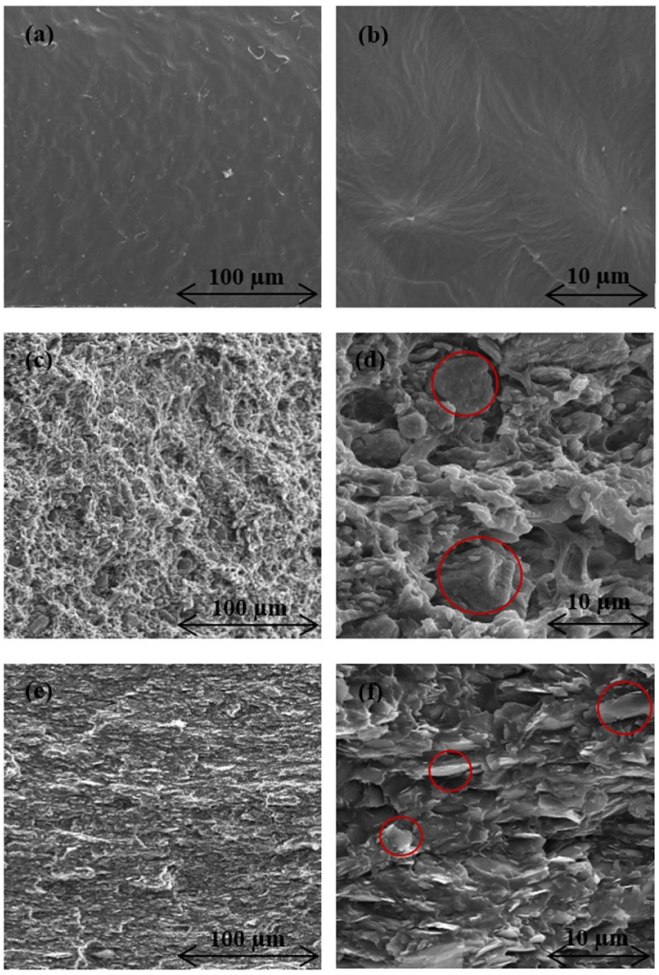

Figure 2. SEM images of the cross-sections of (a) and (b) EPDM, (c) and (d) EPDM$_{CK}$, and (e) and (f) EPDM$_T$.

the EPDM matrix with moderate aggregation. Overall, the EPDM$_{CK}$ looks like a coral morphology. In contrast, the distribution of platelet Talc fillers in the EPDM is more even and without much aggregation, as shown in figures 2(e) and (f). The filler type and composition were further registered and identified by the energy dispersive x-ray spectroscopy (EDXS), as marked for example in figure 2(d) the aggregated Kaolin clay particles and in figure 2(f) the 2D platelet Talc clay nanoparticles. The x-ray mapping of EPDM$_T$ has been shown in figure 3. The EDXS was performed for the area shown in figure 3(a) and the EDX spectrum was presented in figure 3(b). The results from EDX spectrum confirm the presence of Si and Mg from the Talc nanoparticles in EPDM polymer. In addition, the figures 3(c)–(f) present the homogenous distribution of the elements including C, O, Mg, and Si in EPDM$_T$.

The space charge has been measured at two thermal conditions including ambient temperature of 25 °C and ambient temperature of 50 °C, both with a thermal gradient (TG) of 1 °C mm^{-1} across the thickness of the specimen. To provide TG, four resistance heaters were incorporated on the bottom electrode to generate sufficient and laterally uniform thermal gradient across the thickness. Figure 4 presents the evolution of space charge (density) distribution for the three specimens under 20 kV mm^{-1} at 25 °C and 50 °C with 1 °C mm^{-1} TG, respectively, over the initial period of 180 min. Moreover, figure 5 depicts the same results for the three specimens at three determined times of 60, 120, and 180 min. The amount and position of charge accumulation can be seen more clearly in figure 5. In this figure, the charge at the interface of cathode-dielectric and anode-dielectric were presented by negative and positive Gaussian functions, respectively.

For the pure EPDM shown in figures 4(a) and 5(a), the distribution of charge near the cathode-dielectric interface indicates the accumulation of positive charges with an amplitude of 4 C m^{-3} at 25 °C. As shown in figures 4(b) and 5(b), at temperature of 50 °C with TG, these hetero-charges appear to extend sporadically across the sample with near the cathode density increased up to 12 C m^{-3} at time approaching 180 min. In addition, homo-charges are presented at both electrode-dielectric interfaces, with the negative charge density at the cathode-dielectric interface reaching −34 C m^{-3} and the positive charge at the anode-dielectric interface extending approximately 20 C m^{-3}. It should be mentioned that the three vertical lines around 72, 122, and 160 min are the artificial lines created by the measuring PEA technique and signal processing, and they are not valid for interpretation.

For space charge distribution in EPDM$_{CK}$ shown in figures 4(c) and (d), a large amount of homo-charges are detected near both electrodes. At 25 °C, the charge density of accumulated negative homo-charges next to the cathode reaches 2.5 C m^{-3} after 180 min as shown in figure 5(c). At 50 °C

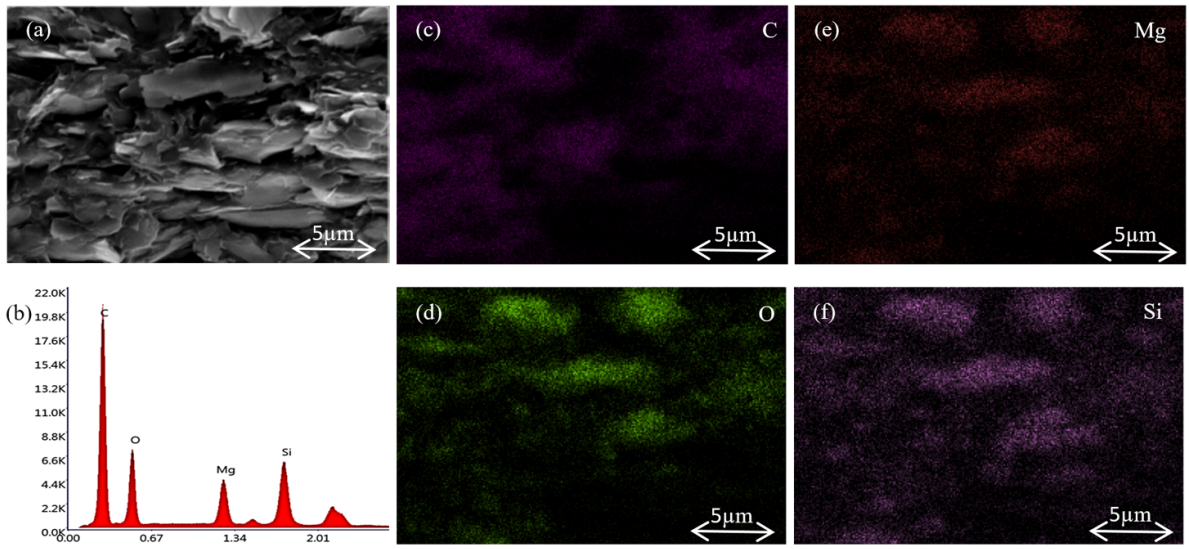

Figure 3. EDXS for the sample $EPDM_T$: (a) SEM images of the cross-sections of the studied area, (b) EDX spectrum, and the elemental mapping of (c) C, (d) O, (e) Mg, and (f) Si.

with TG, the amounts of accumulated charges at the electrode-dielectric interfaces for both electrodes decrease; however, two significant clusters of homo-charge with the maximum charge density of -12.4 C m^{-3} and 10 C m^{-3} were found at a short distance away from the cathode and the anode, respectively. It is interesting to note that, as shown in figures 4(e) and (f), homo-charge and hetero-charge at 25 °C and 50 °C with TG are both suppressed significantly in $EPDM_T$, with the maximum charge density amplitude of only 3 C m^{-3} at 50 °C with TG.

Figure 6 represents the electric field distribution of the three samples after being biased under 20 kV mm^{-1} for 180 min at 25 °C and 50 °C with TG, respectively, and the corresponding evolution of the maximum electric field during the 180 min. Due to the hetero-charge accumulation, the pure EPDM has the highest electric field distortion among the three, with the near cathode maximum values of 32 kV mm^{-1} and 36.6 kV mm^{-1} for 25 °C and 50 °C with TG, respectively. These values correspond to 60% and 83% electric field enhancements over the nominal electric field of 20 kV mm^{-1}. For $EPDM_{CK}$, the peak electric field reached 23.9 kV mm^{-1} for 25 °C and 31 kV mm^{-1} for 50 °C with TG, which represent 19.5% and 55% electric field enhancement over the uniform electric field distribution. Moreover, the location of maximum electric field shifts to the middle of sample, as a result of hetero-charge suppression and homo-charge accumulation. In sharp contrast, due to the excellent space charge suppression property of $EPDM_T$, the maximum electric field for $EPDM_T$ is only 20.7 kV mm^{-1} at 25 °C and 21.6 kV mm^{-1} at 50 °C with TG, resulting in a less than 8% distortion of the nominal electric field, exhibiting a nearly perfect DC performance.

Figure 6(c) shows that the maximum electric field for EPDM and $EPDM_{CK}$ at 25 °C enhances over time especially for the first 90 min and becomes stable during the second 90 min. At 50 °C with TG as shown in figure 6(d), the maximum electric field of both $EPDM_{CK}$ and EPDM increases nearly two times of those at 25 °C, with similar trending except for the slight reduction for EPDM over the second half. In comparison, $EPDM_T$ maintains a stable maximum electric field that is nearly the same as the nominal field of 20 kV mm^{-1} during 180 min for both 25 °C and 50 °C with TG, which shows its superior resistance to space charge accumulation.

The electrical conductivity of samples under 10, 20, 30, and 40 kV mm^{-1} at 25 °C and 50 °C were presented in figure 7. The electrical conductivity of all samples increases with electric field and temperature. The conductivity of $EPDM_{CK}$ and $EPDM_T$ are higher than EPDM under electric field less than 30 kV mm^{-1}. However, it should be emphasized that the electric field dependency was decreased for the filled samples especially the $EPDM_T$ at both temperatures, compared to EPDM with the highest electric field dependency in the range of 10–40 kV mm^{-1} at 50 °C. In other words, although $EPDM_T$ has higher electrical conductivity compared to the other samples, it has the least dependency of conductivity to electric field.

For DC cable insulation, the invariant conductivity with electric field and temperature is desirable [2]. The temperature-dependent part of conductivity follows an Arrhenius relationship:

$$\sigma(T) = \sigma_0 \exp\left(\frac{-\varphi}{kT}\right) \tag{1}$$

where σ_0 is the conductivity at reference temperature (S m^{-1}), φ is the activation energy (eV), k is the Boltzmann's constant (eV K^{-1}), 8.617×10^{-5} (eV K^{-1}), and T is the absolute temperature (K). Figure 8 demonstrates the conductivity of samples under electric field of 10 kV mm^{-1} at 30, 50, 70, and 90 °C. From fitting the conductivity with Arrhenius relationship at low electric field, activation energy of the samples can be obtained, i.e. activation energy

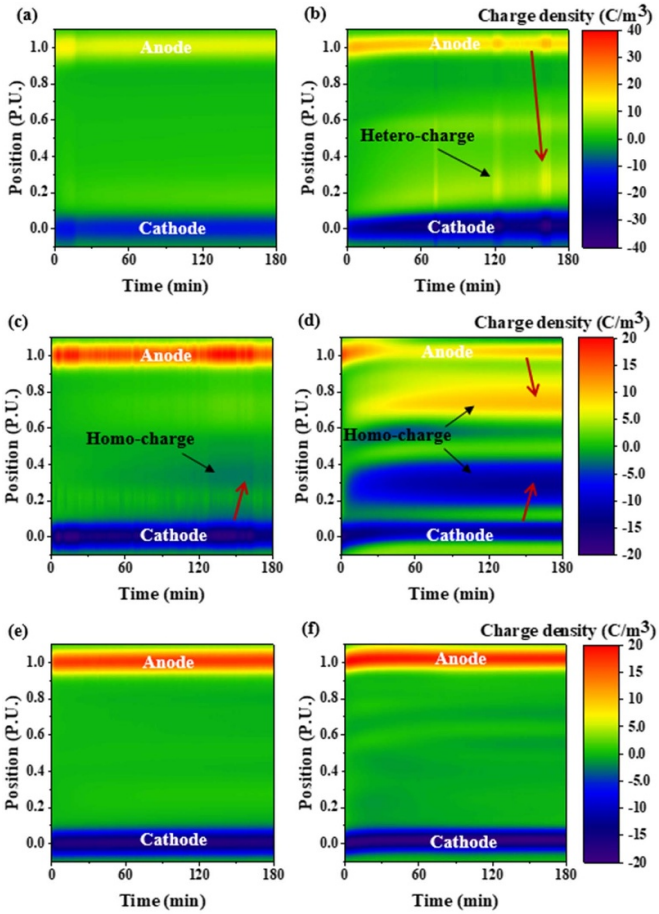

Figure 4. Space charge density distribution across the samples at 20 kV mm^{-1}. (a) EPDM at 25 °C, (b) EPDM at 50 °C with TG, (c) EPDM$_{CK}$ at 25 °C, (d) EPDM$_{CK}$ at 50 °C with TG, (e) EPDM$_{T}$ at 25 °C, and (f) EPDM$_{T}$ at 50 °C with TG. The red arrows show the injected charges from the electrodes.

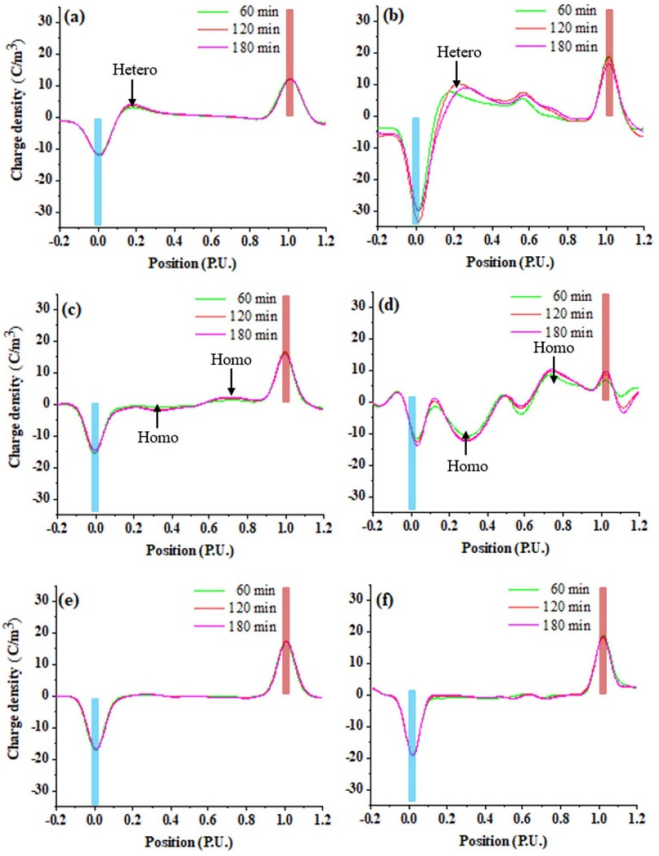

Figure 5. Space charge density distribution across the samples at 20 kV mm^{-1}. (a) EPDM at 25 °C, (b) EPDM at 50 °C with TG, (c) EPDM$_{CK}$ at 25 °C, (d) EPDM$_{CK}$ at 50 °C with TG, (e) EPDM$_{T}$ at 25 °C, and (f) EPDM$_{T}$ at 50 °C with TG. Hetero: hetero-polar charge, and Homo: homo-polar charge.

of 1.27 eV, 0.88 eV, and 0.39 eV for EPDM, EPDM$_{CK}$ and EPDM$_{T}$, respectively. EPDM$_{T}$ has the lowest activation energy of 0.39 eV while EPDM has the highest one with 1.27 eV.

It is important to mention that the power density of a cable insulation is controlled by DC conductivity and electric field. An increase in DC conductivity can lead to the power density enhancement [6]. Therefore, a constraint should be placed in the conductivity enhancement for the filled specimens, EPDM$_{CK}$ and EPDM$_{T}$, to avoid thermal runaway. In addition, a higher activation energy can contribute to the higher conductivity enhancement due to a temperature rise. As a result, these considerations regarding the electrical conductivity should be studied when a particular cable insulation is designed.

Figure 9 depicts the average DC breakdown strength of samples at 25 °C, which are 233, 221, and 252 kV mm^{-1} for EPDM, EPDM$_{CK}$ and EPDM$_{T}$, respectively. In addition, the standard deviation of breakdown strengths has been indicated by a black error bar. An improvement in DC breakdown strength for EPDM$_{T}$ over EPDM can be observed, i.e. an increment of 8%.

To measure the TSDC, the sample was heated to 80 °C and polarized at 20 kV mm^{-1} for 90 min. Then, with the electric field still applied, the sample was cooled to −80 °C. Finally, it was short-circuited and reheated with a rate of 3 °C min^{-1} up to 120 °C. The depolarization currents during the heating as a function of temperature have been shown in figure 10. A significant difference between TSDC of the samples can be observed. The depolarization current of the pure EPDM without filler starts to rise from 55 °C and reaches a single peak of 5 × 10^{-11} A at 100 °C. The initial rise temperature for the composite samples is at a lower temperatures compared with EPDM. EPDM$_{CK}$ showed at least two peaks at 94 °C and 100 °C. The peak at 94 °C reached 9.8 × 10^{-11} A. EPDM$_{T}$ had higher amount of depolarization current at lower temperatures compared with EPDM$_{CK}$ with multiple peaks. The highest peak is at 51 °C with the amplitude of 1.5 × 10^{-10} A. Also, a peak at 92 °C with the amplitude of 9 × 10^{-11} A can be seen which is close to the peak of EPDM$_{CK}$ at 94 °C.

4. Discussion

The results of space charge profiling exhibit that the cross-linked EPDM without any inorganic filler could capture

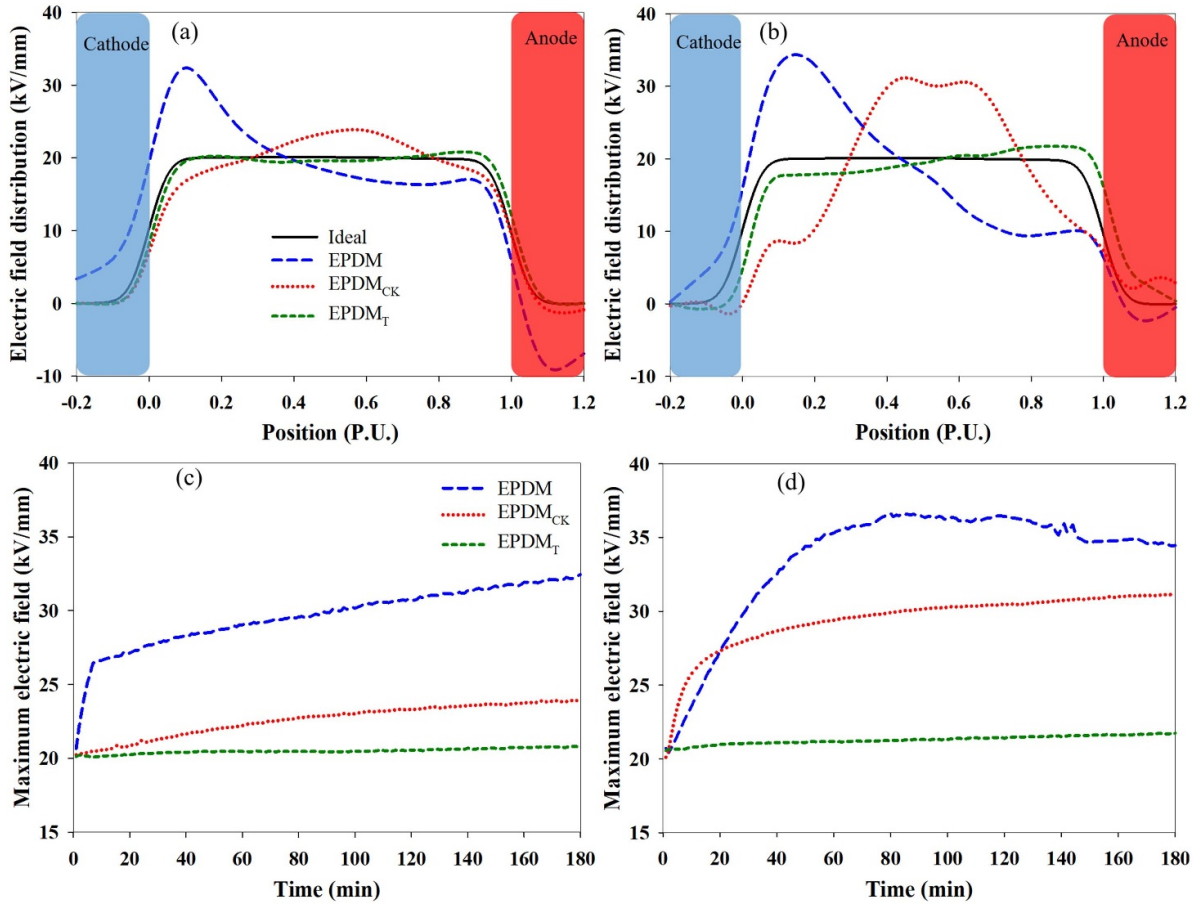

Figure 6. Electric field distribution across the samples after 180 min polarization under 20 kV mm^{-1} (a) at 25 °C, (b) at 50 °C with TG, and the evolution of maximum electric field during 180 min (c) at 25 °C, and (d) at 50 °C with TG.

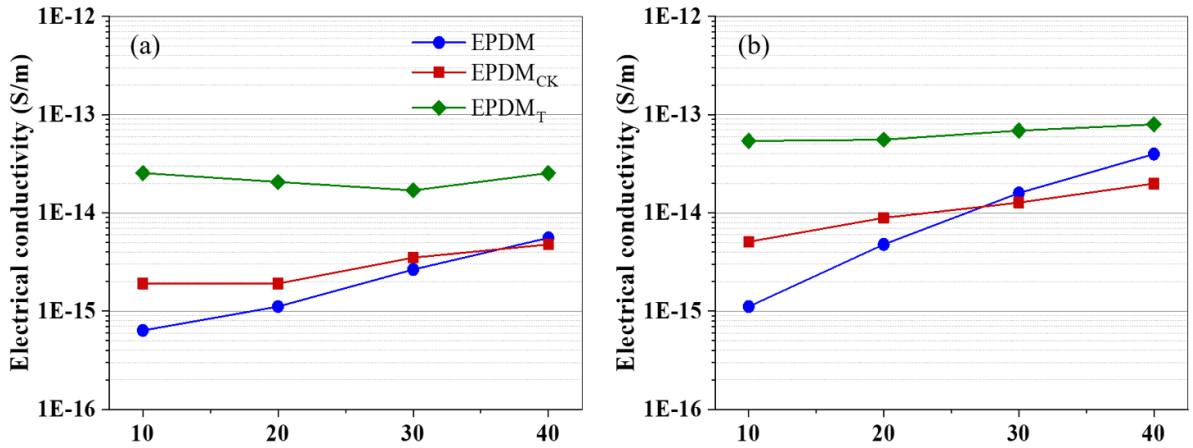

Figure 7. Electrical conductivity under four different electric fields including 10, 20, 30, and 40kV mm^{-1} at (a) 25 °C and (b) 50 °C.

positive charge across the sample and particularly at 50 °C with TG lead to the formation of hetero-charges next to the cathode. Considering the evolution of charge at the electrode-dielectric interfaces of cathode and anode, it appears that the positive charge injected from anode moved across the sample under DC electric field towards the cathode and accumulated in certain locations as depicted in figure 4(b) with the red arrow. Hetero-charge accumulation next to the electrodes is destructive because it could lead to the local electric field enhancement next to the electrode-dielectric interfaces. In addition, the maximum electric field across the cylindrical DC cable insulation occurs next to the anode and cathode due to the dependence of conductivity to electric field and temperature. As a result, this local electric field enhancement due to the hetero-charge superimposes on the Laplacian field next to the electrodes could result in the degradation of dielectric.

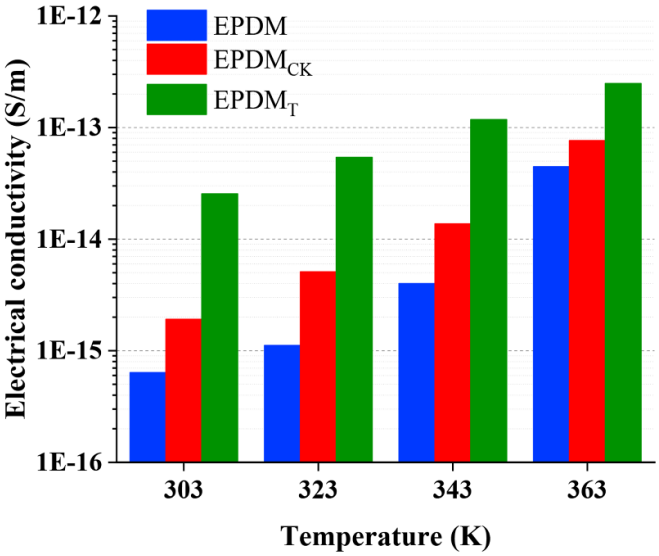

Figure 8. Electrical conductivity at different temperatures under 10 kV mm^{-1}.

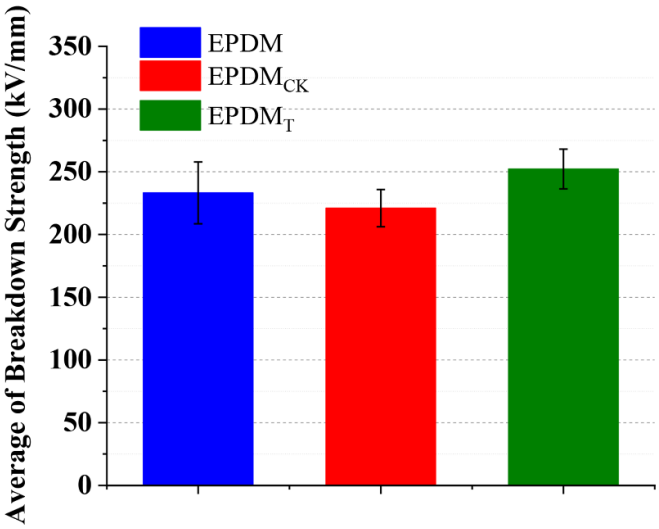

Figure 9. DC breakdown strength at 25 °C.

Introducing 2D clay particles to EPDM matrix suppressed the hetero-charge next to the cathode. However, two clays investigated had different effects on space charge accumulation. EPDM$_{CK}$ presented a high amount of accumulated homo-charge especially at 50 °C with TG. The injected positive charge from anode and negative charge from cathode under DC electric field moved and were trapped next to the homo-polar electrodes as shown with the red arrows in figure 4(d). On the other hand, the EPDM$_T$ could suppress both of the homo-charge and hetero-charge accumulations significantly. The improvement in short-term breakdown strength of EPDM$_T$ also could be related with its ability of in suppression of charge accumulation inside of the bulk under DC electric field. In contrast, the lower breakdown strength of EPDM and EPDM$_{CK}$ could be connected with the higher charge accumulation of these samples.

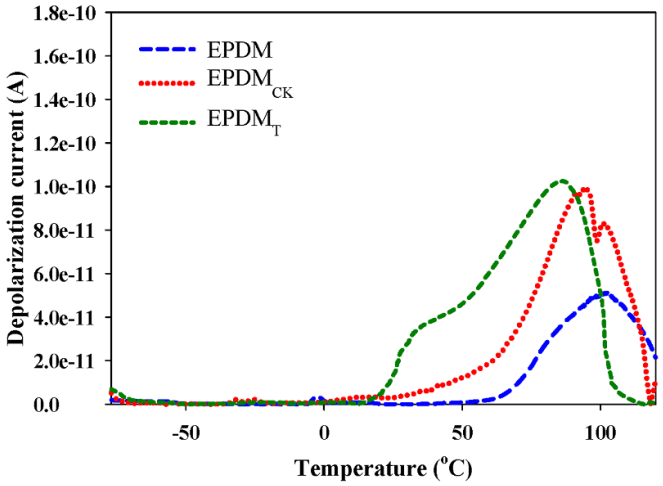

Figure 10. TSDC spectra of the samples polarizing at 20 kV mm^{-1}.

From the experimental results of space charge, it appears that the injected charge at the electrode-dielectric interface has a significant contribution on providing charge carriers. However, the intrinsic charge carriers by donor/acceptor states cannot be neglected in conduction study. Charge transport in the large bandgap dielectrics such as EPDM takes place in the form of conduction through the localized states or traps between the conduction band and valence band of the polymer chains. The average depth of localized states (from so called mobility edges) and the mean distance between localized states which shows as the density of localized states determine the electrical conductivity [6, 17]. Regarding charge transport in the localized states, two major phenomena can happen. The first is hopping through the localized state by movement of a charge carrier from a state to the neighboring one via tunneling through the barriers [18, 19]. The conductivity due to the hopping between the localized states, σ_{hop}, is in relationship with the activation energy for hopping through the states, w, and the average distance between the states, R, as presented in (2) [20, 21];

$$\sigma_{hop} \propto exp\left(-\alpha R - \frac{W}{kT}\right) \tag{2}$$

where α is a constant. The (2) states that increasing the number of localized states enhances the conduction of charge carrier by hopping process.

The other charge carrier transport process is the multiple trapping in which the charge carriers receive enough energy to reach the conduction band and then recaptured by traps. This will happen many times up to the time that the charge carrier reaches the opposite electrode. The conductivity due to the multiple trapping, σ_{multi}, is in relationship with the depth of traps as (3) [21]:

$$\sigma_{multi} \propto \exp\left(-\frac{E_C - E_T}{kT}\right) \tag{3}$$

where E_C is the energy of the conduction band and E_T is the energy level of the trap. The (3) indicates the shallower the

localized states, the higher the conductivity is due to multiple trapping.

Disorders including morphological defects and chemical defects cause the modification of the localized states. The amorphous polymers such as EPDM are considered as highly disordered materials. However, the presence of 2D clays in the composite dielectric modifies the localized states by introducing both morphological and chemical defects. The depth and density of the localized states due to the addition of fillers are dependent on the filler dispersion across the polymer matrix, local interaction of particles with the polymer matrix, the change of morphology due to the presence of particles, etc [22–24]. The base polymer, EPDM, has a different tendency for coating the filler surface, in which this tendency is dependent on the filler type, shape, size and possible modifications on the surface [25]. Considering the SEM photos in figures 2(d) and (f), $EPDM_T$ which is the EPDM filled with Talc particles exhibits a more uniform morphology compared to $EPDM_{CK}$.

This difference of clays distribution in a polymer matrix is dependent on the clays structure and the possible surface modification on it. Clays often have a net negative charge inherently because of the substitution of Si^{+4} with Al^{+3} and Al^{+3} with Mg^{+2} in the structure of clay layers. This negative charge attracts the cations such as Ca^{+2} and Na^{+}. These cations can be shared between two platelet clays, causing aggregation of layers. For a given clay, the number of cations which can be attracted is constant and known as the cation exchange capacity (CEC). Talc has a lower level of CEC compared with Kaolin which prevents Talc particles from aggregation and leads to its great distribution across the polymer matrix [26, 27]. This uniform distribution causes $EPDM_T$ to have a larger interfacial area between the EPDM matrix and clay particles compared to $EPDM_{CK}$ at the same weight ratio filler. The difference in particle distribution across the EPDM matrix for two clays and dissimilar interfacial area between the particles and the EPDM matrix are effective on the distribution of localized states in $EPDM_T$ and $EPDM_{CK}$.

Blaise presented that the high rate of morphological disorder introduces a high number of shallow traps in the polymer chain and enhances the mobility of charge carriers. Detail analytical derivation is beyond the scope of this paper and can be found directly in [21]; however, the result is qualitatively utilized in this study. In figure 5, it was shown that the electrical conductivity of the EPDM with clays are higher than the pure EPDM. The presence of clay particles provides interfacial regions between the EPDM matrix and clay particles. The interfacial area causes the modification of the dielectric's morphology and the introduction of the new shallow traps in the bandgap. Therefore, the enlargement of the interfacial regions can enhance the electrical conductivity of polymeric insulation which is in agreement with the results of [28–31]. As a result, because of the presence of larger interracial area between EPDM and the distributed 2D platelet Talc particles, $EPDM_T$ has higher conductivity than $EPDM_{CK}$ and EPDM. In addition, the higher conductivity of $EPDM_{CK}$ compared to EPDM is due to the presence of interfacial area between the Kaolin particles and the EPDM polymer chains.

Moreover, the presence of 2D clays in the composite dielectric could be considered as chemical disorder with introducing new bonds and interactions at the interface of polymer chains and the filler particles. The depth of traps in these locations are in relationship with the difference between the bandgap of the polymer and the filler [32]. EPDM with fully saturated σ-binding main chain has a bandgap of ∼6–7 eV [33]. The difference between bandgap of EPDM with Kaolin, which has a bandgap of 4.52 eV [34], is higher than Talc particles with a bandgap of 5.3 eV [35]. Therefore, the higher bandgap difference between the polymer and the filler in $EPDM_{CK}$ can possibly cause the deeper traps in this composite compared to $EPDM_T$.

The calculated activation energies by fitting the electrical conductivity results with Arrhenius relationship are 1.27 eV, 0.88 eV, and 0.39 eV for EPDM, $EPDM_{CK}$ and $EPDM_T$, respectively. The activation energy can be interpreted as the average of barrier against transporting charge carriers. It means that $EPDM_T$ with 0.39 eV has the least potential barrier during movement of charge carriers and EPDM has the highest potential barrier with 1.2 eV. In addition, the dependence of conductivity to electric field is in relationship with the trap distribution in the bulk. The separation between two traps is in relationship with electric field dependence of conductivity [30]. The larger distance between two traps causes the higher electric field dependence. The electric field dependence of $EPDM_T$ is lower than $EPDM_{CK}$ and EPDM has the highest electric field dependence among the three materials as presented in figure 5. This can be interpreted as that the trap distribution in the polymer chain of $EPDM_T$ has higher density with shorter average of trap separation compared with $EPDM_{CK}$ and EPDM.

Based on the discussed results of space charge and electrical conductivity, the possible trap distributions of the samples were depicted in figure 11. The cross-linked EPDM sample, as in figure 11(a), has a distribution of traps between the highest occupied molecular orbitals (HOMOs) and the lowest unoccupied molecular orbitals (LUMOs) including both shallow and deep ones. Introducing the 2D clay particles to EPDM matrix increased the amount of shallow traps in both of $EPDM_{CK}$ and $EPDM_T$, as shown in figures 11(b) and (c). As discussed, the shallow traps are responsible mainly for the conductivity in polymeric insulations and this is the reason of the enhanced electrical conductivity for both $EPDM_{CK}$ and $EPDM_T$. The presence of the interfacial area between the EPDM matrix and 2D clays and increasing the morphological disorder are the reasons for the enhancement of the shallow traps. The growth of shallow traps in $EPDM_T$ is significantly higher than $EPDM_{CK}$ because of the higher interfacial area between the platelet Talc particles and EPDM compared to the aggregated Kaolin particles and EPDM. As a result, the density of shallow traps was schemed differently for the three samples with higher density for $EPDM_T$ compared to $EPDM_{CK}$.

The density of deep traps that causes space charge accumulation [36] is not altered similarly in $EPDM_{CK}$ and $EPDM_T$. The higher difference between bandgaps of Kaolin and EPDM

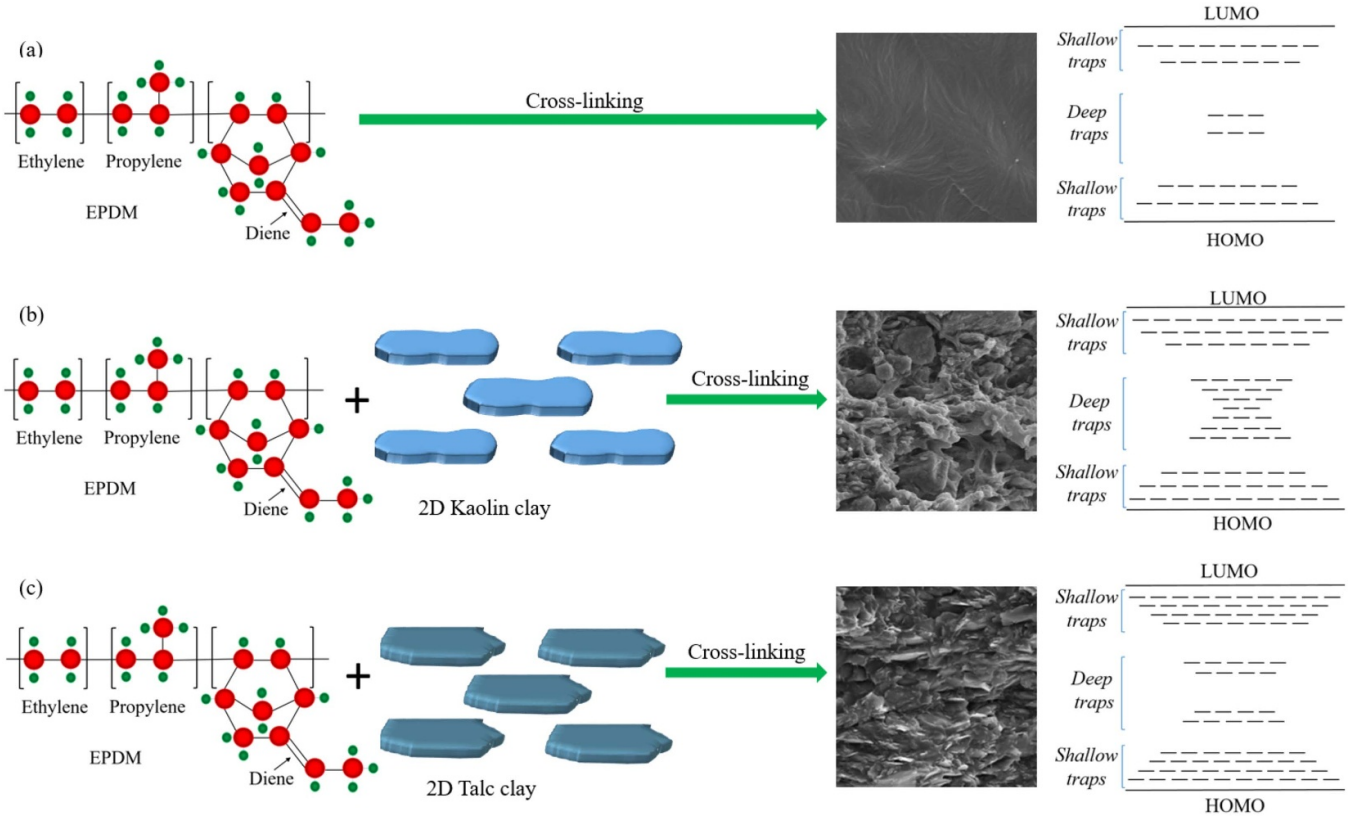

Figure 11. Schematic representation of preparing the samples and the trap distribution for the samples: (a) EPDM, (b) $EPDM_{CK}$, and (c) $EPDM_{T}$.

compared with bandgaps of Talc and EPDM increase the depth of deep traps for $EPDM_{CK}$. This is in good agreement with the space charge density profiling results that show $EPDM_{CK}$ captured the moving charge carriers close to the homo-polar electrodes during the transportation across the sample under electric field. Also, this is in agreement with results of other research such as in literature [37], which states that uniform distribution of particles in polymer matrix decreases space charge accumulation and aggregation of the particles act as charge traps and capture charge carriers during charge transport.

The results of TSDC support the schemed density of states in figure 10. In TSDC method, the initial rise temperature of the depolarization current corresponds to the thermal activation of the trapped carriers. Therefore, the TSDC current at lower temperatures of the spectrum presents the released charge of the shallower traps. The pure EPDM presented the broad peak at temperature about 100 °C. The depolarization current of $EPDM_{CK}$ starts to increase from the lower temperatures and the amplitude of its peaks are higher than the pure EPDM at the same range of temperature. The higher amplitude of depolarization current can be interpreted as the higher density of traps, so it represents that the density of traps for $EPDM_{CK}$ is higher compared to the pure EPDM. The spectrum of $EPDM_{T}$ showed the multiple peaks with high amplitude of current compared to $EPDM_{CK}$ at temperatures lower than 83 °C. Therefore, it can be stated that $EPDM_{T}$ has significantly higher density of shallow traps, in comparison with $EPDM_{CK}$. Also, at higher temperatures, it has only one of the peaks of $EPDM_{CK}$ at about 92 °C. It can be interpreted as the lower average of depth for deep traps in $EPDM_{T}$ compared to $EPDM_{CK}$.

5. Conclusion

In summary, effects of Kaolin and Talc clays on electrical properties of the EPDM-base composite dielectrics were investigated by means of space charge measurement, electrical conductivity, DC breakdown strength, and TSDC. Adding inorganic 2D clays modified the distribution of the localized states and enhanced the electrical conductivity. The EPDM-base polymer filled with Talc particles showed higher conductivity compared to EPDM filled with Kaolin because of the presence of larger interfacial area and possible modification of the interface properties. Moreover, it presented large improvement of space charge suppression and breakdown strength compared to the EPDM and $EPDM_{CK}$. The platelet Talc particles distribute in the EPDM matrix uniformly and leads to a desirable trap distribution with high density of shallow traps and low density of deep traps, which reduced the charge accumulation across the $EPDM_{T}$. Due to this improvement, the maximum local electric field enhancement is decreased from 32 kV mm^{-1} and 36.6 kV mm^{-1} for the pure EPDM at 25 °C and 50 °C with TG, respectively, to 20.7 kV mm^{-1} and 21.6 kV mm^{-1} for the EPDM filled with Talc. The results of

this study thus provide a great guidance for tailoring the novel EPDM-base polymeric insulation for DC cable application.

Data availability statement

The data generated and/or analysed during the current study are not publicly available for legal/ethical reasons but are available from the corresponding author on reasonable request.

Acknowledgments

This work was supported by Kerite, Okonite, Electrical Cable Compounds, Lion Elastomers and Exxon Mobil. The authors thank JoAnne Ronzello for help with the experimental setting-up.

ORCID iD

Yang Cao https://orcid.org/0000-0001-7034-2792

References

[1] Cox P, Fleming R, Krajick F, Boggs S and Cao Y 2016 AC and impulse performance of medium voltage ethylene propylene-rubber cables with over 25 years of in-service aging in a wet underground environment *IEEE Electr. Insul. Mag.* **32** 24–8
[2] Arab Baferani M, Li C, Shahsavarian T, Ronzello J and Cao Y 2021 High temperature insulation materials for DC cable insulation—Part I: space charge and conduction *IEEE Trans. Dielectr. Electr. Insul.* **28** 223–30
[3] Zhou Y, Li Q, Dang B, Yang Y, Shao T, Li H and Wang Q 2018 A scalable, high-throughput, and environmentally benign approach to polymer dielectrics exhibiting significantly improved capacitive performance at high temperatures *Adv. Mater.* **30** 49
[4] Men R, Lei Z, Han T, Fabiani D, Li C, Vincenzo Suraci S and Wang J 2019 Effect of long-term fluorination on surface electrical performance of ethylene propylene rubber *High Volt.* **4** 339–44
[5] Li C, Zhu Y, Hu J, Li Q, Zhang B and He J 2021 Charge cluster triggers unpredictable insulation surface flashover in pressurized SF6 *J. Appl. Phys.* **54** 015308
[6] Tefferi M, Arab Baferani M, Uehara H and Cao Y 2020 The correlation and balance of material properties for DC cable insulation at design field *IEEE Access* **8** 187840–7
[7] Pleşa I, Noţingher P V, Stancu C, Wiesbrock F and Schlögl S 2018 Polyethylene nanocomposites for power cable insulations *Polymers* **11** 24
[8] Roy M, Nelson J K, MacCrone R K and Schadler L S 2007 Candidate mechanisms controlling the electrical characteristics of silica/XLPE nanodielectrics *J. Mater. Sci.* **42** 3789–99
[9] Lau K, Vaughan A, Chen G, Hosier I, Holt A and Ching K 2014 On the space charge and DC breakdown behavior of polyethylene/silica nanocomposites *IEEE Trans. Dielectr. Electr. Insul.* **21** 340–51
[10] Cheng Y, Bai L, Yu G and Zhang X 2018 Effect of particles size on dielectric properties of nano-ZnO/LDPE composites *Materials* **12** 5
[11] Wang Y, Wang C and Xiao K 2016 Investigation of the electrical properties of XLPE/SiC nanocomposites *Polym. Test.* **50** 145–51
[12] Zha J, Dang Z, Song H, Yin Y and Chen G 2010 Dielectric properties and effect of electrical aging on space charge accumulation in polyimide/TiO_2 nanocomposite films *J. Appl. Phys.* **108** 094113
[13] Pallon L K H, Hoang A T, Pourrahimi A M, Hedenqvist M S, Nilsson F, Gubanski S, Gedde U W and Olsson R T 2016 The impact of MgO nanoparticle interface in ultra-insulating polyethylene nanocomposites for high voltage DC cables *J. Mater. Chem.* A **4** 8590–601
[14] Wang S, Zha J, Wu Y, Ren L, Dang Z and Wu J 2015 Preparation, microstructure and properties of polyethylene/alumina nanocomposites for HVDC insulation *IEEE Trans. Dielectr. Electr. Insul.* **22** 3350–6
[15] Zhang C, Zha J, Yan H, Li W, Wen Y and Dang Z 2018 Effects of trap density on space charge suppression of block polypropylene/AI_2O_3 composite under high temperature *IEEE Trans. Dielectr. Electr. Insul.* **25** 1293–9
[16] Wu C, Arab M, Ronzello J and Cao Y 2021 *IEEE Trans. Dielectr. Electr. Insul.* **28** 3–10
[17] Rivnay J, Noriega R, Northrup J, Kline R, Toney M and Salleo A 2011 Charge transport dynamics and space charge accumulation in XLPE composites with 2D platelet fillers for HVDC cable insulation *Phys. Rev.* B **83** 121306
[18] Kübler J and Höck K H 1987 *Hopping Conduction in Solids* ed H Böttger and V V Bryksin (Weinheim, Deerfield Beach-Florida: VCH-Verlagsgesellschaft)
[19] Chiu F 2014 A review on conduction mechanisms in dielectric films *Adv. Mater. Sci. Eng.* **2014** 578168
[20] Stallinga P 2011 Electronic transport in organic materials: comparison of band theory with percolation/(variable range) hopping theory *Adv. Mater.* **23** 3356–62
[21] Blaise G 2001 Charge localization and transport in disordered dielectric materials *J. Electrost.* **50** 69–89
[22] Ma D, Hugener T, Siegel R, Christerson A, Martensson E, Onneby C and Schadler L 2005 Influence of nanoparticle surface modification on the electrical behaviour of polyethylene nanocomposites *Nanotechnology* **16** 724–31
[23] Hosier I, Praeger M, Holt A, Vaughan A and Swingler S 2017 On the effect of functionalizer chain length and water content in polyethylene/silica nanocomposites: part I—Dielectric properties and breakdown strength *IEEE Trans. Dielectr. Electr. Insul.* **24** 1698–707
[24] Alhabill F N, Ayoob R, Andritsch T and Vaughan A S 2018 Introducing particle interphase model for describing the electrical behaviour of nanodielectrics *Mater. Des.* **158** 62–73
[25] Stamhuis J E 1984 Mechanical properties and morphology of polypropylene composites. Talc-filled, elastomer-modified polypropylene *Polym. Compos.* **5** 202–7
[26] Zabihi O, Ahmadi M, Nikafshar S, Preyeswary K and Naebe M 2018 *Composites* B **135** 1–24
[27] Fu S, Sun Z, Huang P, Li Y and Hu N 2019 A technical review on epoxy-clay nanocomposites: structure, properties, and their applications in fiber reinforced composites *Nano Mater. Sci.* **1** 2–30
[28] Lim F, Fleming R and Naybour R 1999 Space charge accumulation in power cable XLPE insulation *IEEE Trans. Dielectr. Electr. Insul.* **6** 273–81
[29] Yan P, Zhou Y and Yoshimura N 2000 DC conduction in polyethylene films under high electric field after annealing *J. Phys. D: Appl. Phys.* **39** 3492–5
[30] Mizutani T, Semi H and Kaneko K 2000 Space charge behavior in low-density polyethylene *IEEE Trans. Dielectr. Electr. Insul.* **7** 503–8

[31] Jeroense M and Kreuger F 1995 Electrical conduction in HVDC mass-impregnated paper cable *IEEE Trans. Dielectr. Electr. Insul.* **5** 718–23
[32] Haneef H F, Zeidell A M and Jurchescu O D 2020 Charge carrier traps in organic semiconductors: a review on the underlying physics and impact on electronic devices *J. Mater. Chem.* C **8** 759–87
[33] Li J, Du B, Su J, Liang H and Liu Y 2018 Surface layer fluorination-modulated space charge behaviors in HVDC cable accessory *Polymers* **10** 500
[34] Xia L, Zhong H, Liu G and Xingang L 2009 Electron bandstructure of kaolinite and its mechanism of flotation using dodecylamine as collector *J. Cent. South Univ. Technol.* **16** 73–79
[35] Alencar A B, Barboza A P M, Archanjo B S, Chacham H and Neves B R 2015 Experimental and theoretical investigations of monolayer and few-layer talc *2D Mater.* **21** 015004
[36] Teyssedre G and Laurent C 2005 Charge transport modeling in insulating polymers: from molecular to macroscopic scale *IEEE Trans. Dielectr. Electr. Insul.* **12** 857–75
[37] Andritsch T 2010 Epoxy based nanodielectrics for high voltage DC-applications: synthesis, dielectric properties and space charge dynamics Doctoral Dissertation Delft University of Technology